Toward Sustainable Electronics: Exploiting the Potential of a Biodegradable Cellulose Blend for Photolithographic Processes and Eco-Friendly Devices

Elena Palmieri, Luca Maiolo,* Ivano Lucarini, Adriano Diaz Fattorini, Emanuela Tamburri, Silvia Orlanducci, Raffaella Calarco, and Francesco Maita

Flexible electronics has emerged as a promising field for the development of electronic devices with applications in wearables, biomedical sensors, and edible electronics. Biomaterials play a crucial role in fabricating flexible substrates, and the utilization of polymer blends offers exciting possibilities for tuning mechanical and chemical properties. This paper highlights the potential of a novel polymer blend based on ethyl cellulose (EC) and hydroxypropyl cellulose (HPC) in the fabrication of substrates for flexible electronics. By blending the two cellulose ethers, it is possible to tune the mechanical and chemical properties of the final substrate, tailored to meet specific requirements. To exploit such innovative green substrates for photolithographic processes, their stability, and processability is extensively investigated. The feasibility of photolithographic processes on such biodegradable and edible substrates is demonstrated by fabricating both resistive and capacitive sensors through standard photolithographic processes, presenting a breakthrough in terms of applicability. The utilization of such biomaterials holds tremendous potential for driving technological advancements in various fields. These materials pave the way for innovative devices catering to diverse applications, from agriculture to food and biomedicine. Importantly, they also promote a sustainable approach for their fabrication, laying the foundation for an environment-aware future of technological progress.

1. Introduction

In the context of flexible electronics, a great effort has been done in the last decades to produce thin, flexible, and performing devices. One of the main issues concerning the fabrication of such devices is the choice of substrate, which is crucial to determine the processability and the potential application and final performances of the devices. In general, high glass transition temperature plastic-based substrates (e.g., polyimide (PI) and Kapton) are still the first choice when it comes to such devices, due to their easy processability, high chemical resistance, and high flexibility.[1,2,3–10,11] Plastic-based substrates do not present any of the limitations typical of biomaterials, which are far less processable, as they show poor resistance to high temperature, chemicals, and a surface roughness not compatible with thin film technology. In fact, standard microfabrication processes are generally not applicable to biomaterials as they involve the use of temperature >200 °C and/or strong chemicals (alkali/acid).

Nevertheless, driven by the pressing environmental crisis, endeavors have been taken to optimize green substrates based on biopolymers (e.g., proteins, cellulose, and their derivatives).[12–15] Unfortunately, substrate optimization often involves the coupling of such biomaterials with hazardous ones, to make them processable and suitable for the fabrication of devices.[16–19] Despite impressive results were achieved,[18,19] some of the limitations of such materials have yet to be overcome. For this reason, the techniques implemented for the fabrication of devices on biomaterial substrate are low temperature processes (T<100 °C), such as screen printing and ink-jet printing[20,21] and coating techniques.[13,22] However, these techniques are not compatible with strong miniaturization and tend to produce medium/high-resistivity layers ($\rho = 1 - 100$ Ωcm) and devices with not uniform performance, that limit their applicability to a reduced range of fields. Furthermore, in contrast to thermal evaporation processes, printing and coating techniques result in the deposition of considerably higher amounts of conductive materials that include

E. Palmieri, L. Maiolo, I. Lucarini, A. D. Fattorini, R. Calarco, F. Maita
Istituto per la Microelettronica e i Microsistemi
Consiglio Nazionale delle Ricerche
Via del Fosso del Cavaliere n.100, Rome 00133, Italy
E-mail: luca.maiolo@cnr.it; ivano.lucarini@cnr.it; francesco.maita@cnr.it
E. Tamburri, S. Orlanducci
Department of Chemical Science and Technologies
University of Rome Tor Vergata
Via della Ricerca Scientifica 1, Rome 00133, Italy

detrimental solvents and chemicals. The increased amounts of metals or conductive materials compromise the overall sustainability of the final device.

One of the biomaterials that has been thoroughly exploited in the last decades is cellulose, in the form of paper sheets, properly customized and functionalized depending on the application, and other cellulose-based derivatives.[13,23–30] More specifically, in the last two decades the production of self-standing substrates for electronics fabricated from Cellulose Nanofibers (CNF) has been optimized.[31] While the advantages of the use of such a substrate are its biodegradability, sustainability, and transparency, its very chemical nature represents a major disadvantage under various aspects. While the hydrophilicity of commonly used cellulose-based substrates could be exploited for the fabrication of humidity sensors,[32,33] it limits greatly their field of application. In fact, the operability of a device based on CNF or other commonly used cellulose-based substrate is impeded outdoors or in any uncontrolled humidity environment. Moreover, the substrates are subject to degradation or swelling if exposed to solvents or water-based materials. For this very reason, devices on CNF sheets are generally fabricated through screen printing or ink-jet printing, as these techniques allow for the deposition of metals or any other conductive materials in a non-destructive way. However, this prevents large-scale adoption of this substrate, as many laboratories and industries rely on standard photolithographic techniques for the fabrication of electronic devices. Alternative approaches, involving the utilization of cellulose-based ionogels, have proven to be effective in serving as adaptable and customizable platforms for electronic devices like electronic skin (e-skin) and wearables.[34–36] Nevertheless, it should be noted that they exhibit sensitivity to moisture and chemicals, which imposes constraints on their applicability in certain scenarios.

Our research work tries to address all these issues focusing on the design and development of a fully biodegradable substrate that can be processed using standard photolithographic techniques. To the best of our knowledge, little research work has been done to investigate the compatibility of cellulose ethers with such processes. The results obtained so far, in fact, involve the use of modified cellulose, synthesized using fluorinated chemicals. The process is performed using organic solvents as chloroform, affecting the overall sustainability of such substrates.[37,38] Another work proposes the use of a functionalized agarose substrate suitable for photolithographic processes.[39] Although these results sound very promising, the functionalization of the agarose and the preparation of the substrate make use of organic solvents and high-hazard materials. Moreover, the substrate functionalized as described is not completely stable, and the substrate requires to undergo photolithography soon after preparation. Our approach does not make use of any organic solvents or high-hazard chemicals to fabricate the substrate, and it might represent a feasible and actually green alternative in the fabrication of flexible electronics through photolithography. The proposed material allows the production of flexible sustainable electronic devices using a technique that, to the best of our knowledge, to date, was restricted to other materials (silicon, glass, PET, PI).[40–42] In years to come, this will support a significative reduction of plastic-based substrates in the next generation of flexible electronics devices while allowing industries to keep using their fabrication lines and the processes that they already had optimized.

Within this framework, we are proposing cellulose-based materials for the fabrication of self-standing substrates for electronics. Two cellulose ethers are used for the preparation of three different formulations, thus three substrates, which are optimized and characterized. More specifically, ethyl cellulose is chosen for its well-established application in the electronic field as a binder and matrix for the preparation of inks and conductive electrodes.[29,43–49] Ethyl cellulose (EC), unlike most cellulose derivatives, is highly hydrophobic, posing a significant advantage for its possible application. In fact, the hydrophobicity of the cellulose-based substrate could prevent its degradation/dissolution due to the chemicals that it is exposed to during the fabrication process of the device. Moreover, its hydrophobicity might widen its field of application to outdoor use as precision agriculture, environment monitoring, smart city scenarios, etc. The other cellulose used in this work is hydroxypropyl cellulose (HPC), which is hydrophilic and has been proven to possess interesting features to be exploited in electronics such as very good filming properties and printability.[16,23,32,50–53]
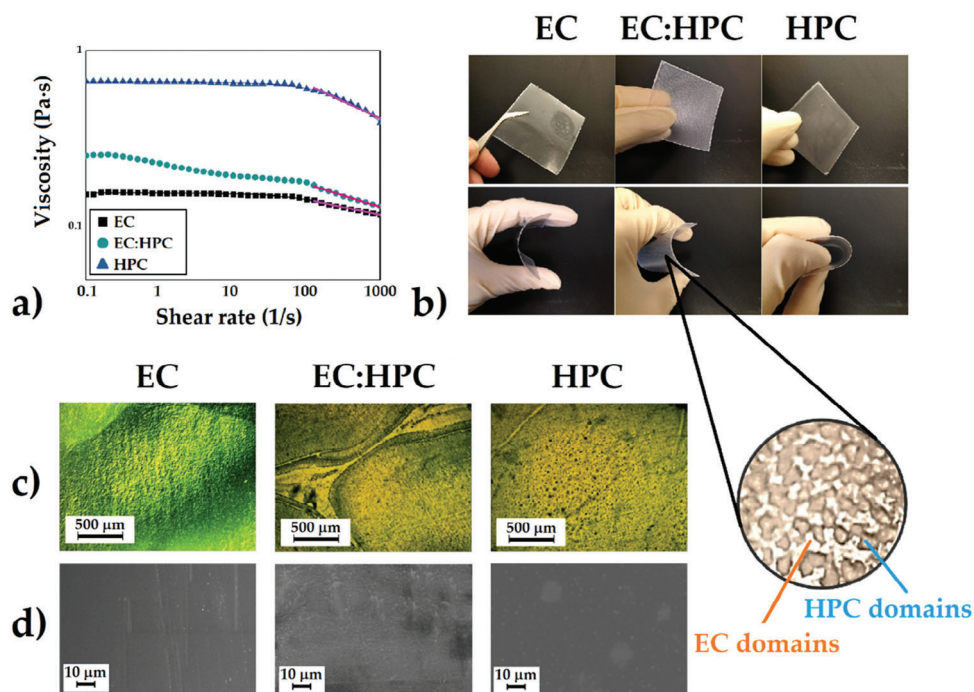
The substrates presented in this work, prepared from three ethanol-based formulations via solvent casting, are characterized to assess their processability toward photo-lithographic processes. By varying the formulation, we prove the possibility to tune the chemical, physical and mechanical properties of the substrate. This allows us to prepare substrates able to fit a wide range of processes, from photolithography to screen printing, while being sustainable, easy to prepare, and not energy consuming. Moreover, the mechanical properties of such substrate are evaluated to assess their exploitation when subjected to strain, such as in devices for wearable electronics and outdoor applications (or precision agriculture, cultural heritage diagnosis and preservation, or environmental monitoring). Finally, Titanium and Aluminum based resistive strain gauge sensors and capacitive humidity sensors are fabricated through standard photolithographic process on such substrates, proving de facto their potentiality and applicability.

2. Results and Discussion

2.1. Materials Characterization

2.1.1. Rheological Measurements

Rheological analyses were conducted on the solutions investigated in this study, i.e., ethyl cellulose (EC), hydroxypropyl cellulose (HPC) and a blend of the two (EC:HPC), to assess the processability of the prepared dispersions, investigating shear rates ($\dot{\gamma}$) ranging from 0.1 to 1000 s^{-1}. We selected a broad shear rate range to not only examine the dispersion's behavior at the shear rate linked to the specific deposition method, i.e., solvent casting, but also to assess its stability under different conditions. The lower end of this range corresponds to storage, film leveling, and low-shear deposition techniques, while the higher shear rates align with typical coating and printing method.[54,55] In general, the shear rate applied to the solution can be estimated according to the process and to the specific set-up. In our case, focusing on solvent casting,[56,57] if the fluid is poured into the mold, the involved shear rate is low, approximately ≈0.1 s^{-1}. However, we opted to transfer the solutions to the mold via a syringe,

**ADVANCED
SCIENCE NEWS**

www.advancedsciencenews.com

**ADVANCED
MATERIALS
TECHNOLOGIES**

www.advmattechnol.de

Figure 1. a) Double logarithmic shear viscosity-shear rate profiles for all the tested formulations. The whole curve for EC and HPC formulations was fitted using the Cross model (black and blue line). The linear region of the curve is fitted using the Power law model (purple lines). b) Pictures of the three cellulose-based films. Inset: detail of the EC:HPC substrate. c) Optical microscope images of EC, EC:HPC and HPC; d) SEM micrographs of EC, EC:HPC and HPC.

providing us with better control over the deposited quantity and consequently the film's thickness. This results in the solutions undergoing a mild extrusion process. The shear rate associated with such extrusion processes can be determined using the Equations 1 and 2.[58–63]

$$\overset{\circ}{\gamma} = (3n + 1)/4n \times 4Q/\left(\pi R^3\right) \tag{1}$$

$$\overset{\circ}{\gamma} = 4Q/\left(\pi R^3\right) \tag{2}$$

where "Q" stands for the volume flow rate, "R" the diameter of the syringe and "n" is a parameter indicating how much the fluid deviates from a Newtonian fluid (n = 1 for Newtonian, <1 for shear-thinning, and >1 for shear-thickening fluids). Therefore Equation 1 is the general formula, while Equation 2 is the simplified one for Newtonian fluids. For our set up, the shear rate applied to the fluid is ≈100 s^{-1} (if we consider it as a Newtonian fluid, slightly lower if calculated using the n derived from rheological tests performed and reported in Table S1, of Supporting Information). The estimated value falls within the shear rate range evaluated.

The viscosity-shear rate profiles of the solutions investigated in this study are reported in **Figure 1a**. Examining the flow curves of ethyl cellulose solution and hydroxypropyl cellulose one can readily discern a reduction in viscosity with increasing shear rates. This behavior is characteristic of shear-thinning fluids, aligning with expectations based on existing literature data,[64–66] although it is worth noting that some studies have reported slightly different responses for both polymers at higher concentrations.[66]

The flow curves were modeled using the Cross model,[67–71] and the linear portion of the graph was fitted using the Power Law relationships. The specific equations and parameters derived from this analysis can be found in the Supporting Information, as listed in Table S1, Equations S1 and S2 (Supporting Information). Within the tested range of shear rates, both solutions exhibited stability, maintaining their characteristic shear-thinning behavior. The hydroxypropyl cellulose (HPC) solution possessed a higher viscosity, albeit still within an acceptable range for achieving uniform film leveling. In the case of the mixed dispersion composed of EC and HPC, some slight deviation from the typical pseudoplastic profiles became apparent and are discussed in Supporting Information. From a qualitative perspective, it is evident that the viscosity of EC:HPC falls between that of the HPC and EC formulations. Regarding the linear region, the parameters derived from the Power Law fitting exhibit an intermediate position between those of HPC and EC, which can be found in Table S1 (Supporting Information).

2.1.2. Optical and Morphological Characterization of Cellulose Films

The cellulose ethers dispersions were solvent cast to render cellulose films of 1.25 ± 0.09 g cm^{-3} for EC, 1.21 ± 0.04 g cm^{-3} for EC:HPC, and 1.28 ± 0.06 g cm^{-3} for HPC.

The films are transparent and very smooth. EC film is translucent, while HPC film is transparent but opaquer (Figure 1b).

As for the EC:HPC film, it presents a pattern due to the presence of the two polymers. In fact, we can clearly observe with the

2301282 (3 of 12)
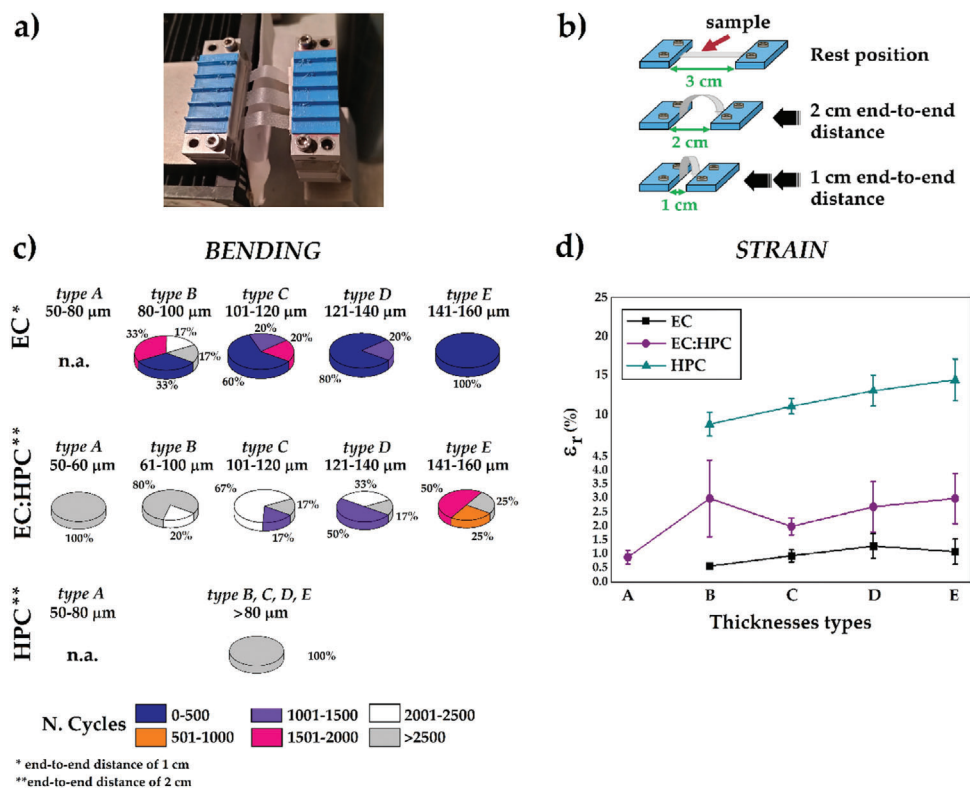
Figure 2. a) Photograph of the bending tests set up; b) Sketch representing the two bending positions investigated; c) Results from bending test for the EC, EC:HPC and HPC substrates, for the five-thickness tested (A, B, C, D and E types). d) Results from strain tests for the EC, EC:HPC and HPC substrates assessed as a function of the thickness (increasing thickness from A type to E type). The maximum strain reached is the material's point of fracture.

naked eye the presence of a translucid matrix (EC) sparkled with opaquer domains (HPC) (Figure 1b, inset).

The morphology of the self-standing films was investigated through optical and scanning electronic microscopy (Figure 1c,d).

Optical microscope images validated the uniformity of the surfaces on both EC and HPC substrates. Conversely, they revealed a distinctive patterned surface in the case of EC:HPC. This surface displayed the presence of two immiscible phases, giving rise to enclosed domains (Figure 1c, middle picture).

SEM analysis depicted relatively smooth surfaces for both the EC and HPC substrates, as illustrated in Figure 1d (left and right picture). The minor flaws observed were primarily attributed to salt residues in the polymer powder, a phenomenon observed in a previous work,[13] as the polymer was employed without purification for the preparation of the substrate. Additionally, handling and peeling-off procedures may have contributed to these imperfections. As for EC:HPC substrate, a less regular surface can be observed (Figure 1d, middle picture). It should be noted that these images are representative of the surface of the substrate in contact with the mold. While for EC and HPC there is no significant difference in morphology between bottom and top side, the EC:HPC has a top surface more irregular and rougher (Figure S1a, Supporting Information), so it is not suitable for metal depositions where high resolution or very thin metal thickness (<100 nm) are required. (Figure S1b, Supporting Information).

2.1.3. Mechanical Properties

The mechanical properties of the thin films were investigated through bending tests and stress-strain tests. Around 30 substrates for each type were tested using the apparatus reported in **Figure 2a**. The samples were subjected to up to 2500 bending cycles, with an initial end-to-end distance of 3 cm, and a position of maximum bending of 1 cm end-to-end distance (bending radius of ≈5 mm) (Figure 2b). For EC also a 2 cm end-to-end distance (bending radius of ≈7 mm) was investigated, given the poor results obtained with the other configuration. The samples showed considerably different mechanical properties depending on the thickness and the chemical composition. As explained in Table 2 of the Experimental Section, the substrates were divided in five classes, from A to E, according to their thickness, from the thinner (A) to the thicker (E).

HPC substrates exhibit stability for over 2500 cycles, regardless of their thickness. In contrast, the mechanical properties of EC:HPC substrates are influenced by their thickness. Thinner samples from groups A and B demonstrated stability over 2000 cycles, with performance levels comparable to HPC substrates. Among the thicker samples (designated as type E), 25% experienced breakage within 1000 cycles, while another 25% endured for over 2500 cycles (as illustrated in Figure 2c). For substrates exceeding 180 μm in thickness (not shown on the graph), material rupture occurred within the initial 100 cycles. In the case of an end-to-end distance of 1 cm, poor results were obtained for

**ADVANCED
SCIENCE NEWS**

www.advancedsciencenews.com

**ADVANCED
MATERIALS
TECHNOLOGIES**

www.advmattechnol.de

the EC substrate. In fact, all the samples broke within five cycles. Therefore, bending tests were performed with a 2 cm end-to-end distance (Figure 2b), showing fair performances (Figure 2c). 33% of substrates from group B showed breaking points within 500 cycles, however a 34% lasted over 2000 cycles. As observed before, the mechanical feature toward bending is clearly dependent on the thickness of the substrate. In fact, all the tested samples from group E broke within 100 cycles.

Strain measurements were performed using the same set-up as for the bending tests. The sample were pulled from an extremity at a speed of 2 mms^{-1} with a step size of 0.05 mm. The relative strain was calculated using Equation 3:

$$\%\varepsilon_r = (\varepsilon - \varepsilon_i)/\varepsilon_i \times 100 \tag{3}$$

Results of the relative strain as a function of the thickness are reported in Figure 2d. For the EC samples, as expected, mediocre results were obtained, showing a maximum strain before breakage of ≈%. For the EC:HPC-based films, better mechanical properties under strain are observed. The maximum strain reached is ≈3%. An improvement with increasing thickness is observed, starting from a 1% strain for the thinner sample (A type), to a 3% strain for the thicker one (E type). However, values are affected by significative error, so differences between B, C, D and E types are not significant.

HPC demonstrated impressive mechanical characteristics, achieving a 15% relative strain in the type E samples. We also conducted tests on both EC:HPC and HPC specimens with thickness exceeding that of type E, reaching a relative strain of ≈25% for HPC (although this data is not displayed on the graph). This substantiates that augmenting the thickness results in a noticeable enhancement in tensile strength, with the maximum thickness assessed being 200 μm.

Consequently, based on the mechanical assessments conducted, EC:HPC exhibited intermediary properties. Specifically, it does not exhibit the brittleness associated with EC nor the same degree of flexibility and elasticity seen in HPC. The incorporation of HPC domains into the EC matrix, emerged from the analysis of optical images of EC:HPC substrates, is the primary contributor to its mechanical characteristics. These regions are likely responsible for imparting greater flexibility and elasticity to the film compared to pure EC.

2.2. Processability Evaluation

With the aim of using such substrates in standard photolithographic procedures it is mandatory to investigate their processability. In fact, during the fabrication of electronic devices, the substrate undergoes solvents and chemicals treatments, coupled with UV radiation at 365 nm for a few minutes. Therefore, to assess the suitability of such substrates to the photolithographic process, they were immersed in common solvents such as deionized water, acetone, and isopropyl alcohol (IPA), and in chemicals used in photolithographic processes, such as liquid/dry photoresists and their developers and strippers. More specifically, the chemicals investigated are the etching solution for Aluminum, MF319, AZ400K (widely used positive photoresist developers), the etching solution for Chromium and the etching for Titanium. We focused on the fabrication of Titanium and Aluminum

Table 1. Response of the various substrates to solvents and chemicals. Legend: √: the sample does not show any visible sign of swelling/degradation; X: the sample starts showing sign of swelling/degradation; Not tested: not tested due to swelling/degradation occurred at lower exposure time.

		30 sec	5 min	15 min	1 hr
HPC	**Water**	√	X	Not tested	Not tested
	Aceton	X	Not tested	Not tested	Not tested
	IPA	X	Not tested	Not tested	Not tested
	MF319	X	Not tested	Not tested	Not tested
	Etching Al	X	Not tested	Not tested	Not tested
	Etching Cr	X	Not tested	Not tested	Not tested
	Etching Ti	X	Not tested	Not tested	Not tested
	AZ400K	X	Not tested	Not tested	Not tested
EC:HPC	**Water**	√	√	√	X
	Aceton	X	Not tested	Not tested	Not tested
	IPA	X	Not tested	Not tested	Not tested
	MF319	√	√	√	X
	Etching Al	√	X	Not tested	Not tested
	Etching Cr	√	√	√	X
	Etching Ti	√	√	X	Not tested
	AZ400K	√	√	√	X
EC	**Water**	√	√	√	√
	Aceton	X	Not tested	Not tested	Not tested
	IPA	X	Not tested	Not tested	Not tested
	MF319	√	√	√	X
	Etching Al	√	X	Not tested	Not tested
	Etching Cr	√	√	√	X
	Etching Ti	√	√	X	Not tested
	AZ400K	√	√	√	X

based devices, as they are the least impactful and most biocompatible metals exploited in the fabrication of electronic devices. Moreover, Aluminum can be etched also using resin developers (MF319 and AZ400K), which gives larger room for processability. We also evaluated the feasibility of etching Chromium, although far from being sustainable and biocompatible, as it can play various roles in the fabrication of a device as sacrificial or adhesion layer, making it a very versatile metal.

The exposure times were established based on the common duration of the treatments and/or according to the first visible signs of deterioration occurring on the samples.

The stability of the substrates toward these chemicals was evaluated by assessing the weight loss, due to degradation, or weight gain due to hydration, by observing change in color, shape, and consistency. Moreover, X-Ray diffraction (XRD), Attenuated Total Reflection-Fourier Transform Infrared Spectroscopy (ATR-FTIR) and UV–vis characterization of the treated substrates samples were performed to further assess their preservation state. In **Table 1** the main results for the various substrates are reported. According to Table 1, all the substrates are unstable toward organic solvents such as acetone and IPA, as they are soluble in such solvents. Moreover, the substrates containing HPC, which is hydrophilic, show a tendency to swell in water, even after a few minutes. Once the substrate is dried, it cannot go back to its

**ADVANCED
SCIENCE NEWS**

www.advancedsciencenews.com

**ADVANCED
MATERIALS
TECHNOLOGIES**

www.advmattechnol.de

original state, and its morphology and shape slightly change. As for the EC, being highly hydrophobic, it is extremely stable in water (we tested its resistance in over 4 months of immersion in water, recording no variation in shape, weight, and morphology), and it is quite stable in all the water-based chemicals, despite their extreme pH.

On the other hand, HPC shows the limitation typical of commonly used cellulose-based substrate. In fact, at extreme pH, it is subject to hydrolysis, which is noticeable by the yellowish color assumed by the sample (Figure S2, Supporting Information).

The mixed EC:HPC substrates, as expected, present intermediate behavior. They show an acceptable resistance to various chemicals, which is sufficient to make it a valid candidate for the fabrication process. No weight variations are recorded for the EC and EC:HPC samples for the treatment and time exposure corresponding to the green-coloured cells in Table 1.

Despite retaining their shape, thickness, and weight, some of the EC:HPC samples showed some variations in their optical features, due probably to the functionalization of the surface operated by the various chemicals tested. EC:HPC samples become opaquer, while EC samples remained unaltered.

Given this preliminary evidence, the EC and EC:HPC substrates treated with the MF319, AZ400K, etching for Chromium, etching for Titanium were further characterized via XRD, and UV–vis and FTIR spectroscopy. Only results regarding the MF319 and the etching for Titanium are reported in the main text, other data are reported in Figure S3, (Supporting Information).

The XRD diffractogram of these substrates showed a very poor crystalline structure. In fact, the cellulose ethers used to prepare the substrate are obtained from alkaline treatment of cellulose, which causes cellulose to lose its crystalline domains. As a consequence, the peaks associated with crystalline cellulose domains (101, 10$\bar{1}$, 021, 002) are lost and a broad peak appears at ≈20°[72,73] that might be assigned to amorphous cellulose. No significative variations are observed among the samples treated with the etching solution for Titanium and MF319, suggesting that the action of these chemicals for the tested times does not induce further amorphizations (**Figure 3a**). FTIR-ATR and UV–vis spectra of the substrate before and after treatment were collected, and results regarding MF319 and etching for Titanium are reported in Figure 3b,c.
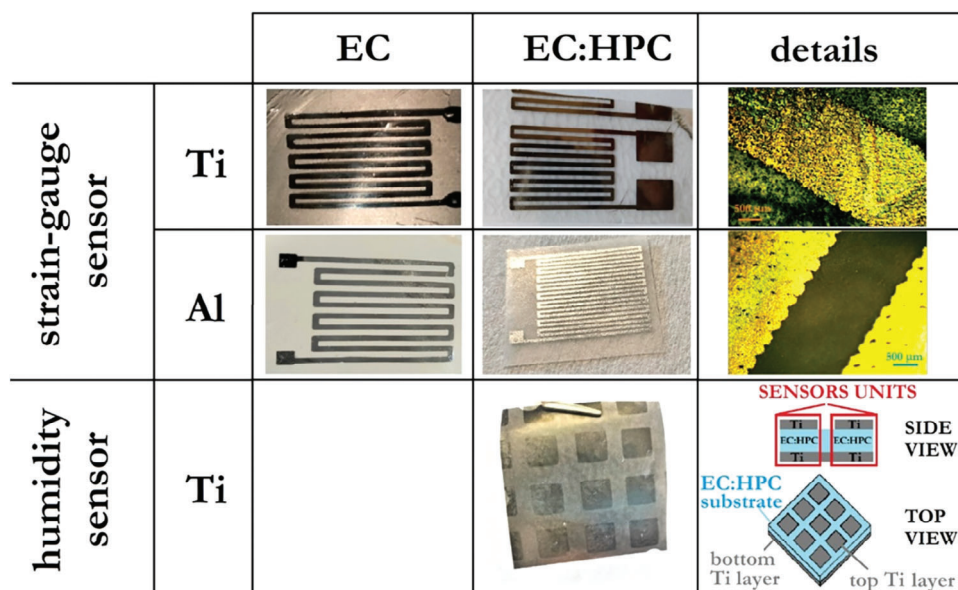
In the FTIR-ATR spectra presented, the bands at ≈3400, 2900, 1430, 1370, 1050 and 900 cm^{-1} are associated to native cellulose. More precisely, the band at 3400 cm^{-1} is associated to the stretching of —OH groups and the band ≈2900 cm^{-1} to the stretching of the C—H bonds. The C—O—C of the pyranose ring vibrations contributes to the peak at ≈1050 cm^{-1}, while the peak at ≈1370 cm^{-1} is associated to the C—H bending.[74–76] The complex band from 1200 to 1500 cm^{-1} is due to the bending of the C—H groups, while the band from 500 to 800 cm^{-1} is associated to the OH out of plane bending. No significative difference is observed among the EC, EC:HPC and HPC samples (pristine), except for the 3400 cm^{-1} band, due to the hydroxylic groups present on the side chain of HPC. A red shift of this band is observed for HPC, which is due to the development of stronger hydrogen bonds with respect to EC. Moreover, the 1650 cm^{-1} band originated by the —OH bending of absorbed water molecules, is more evident in the HPC substrate (hydrophilic) with respect to the
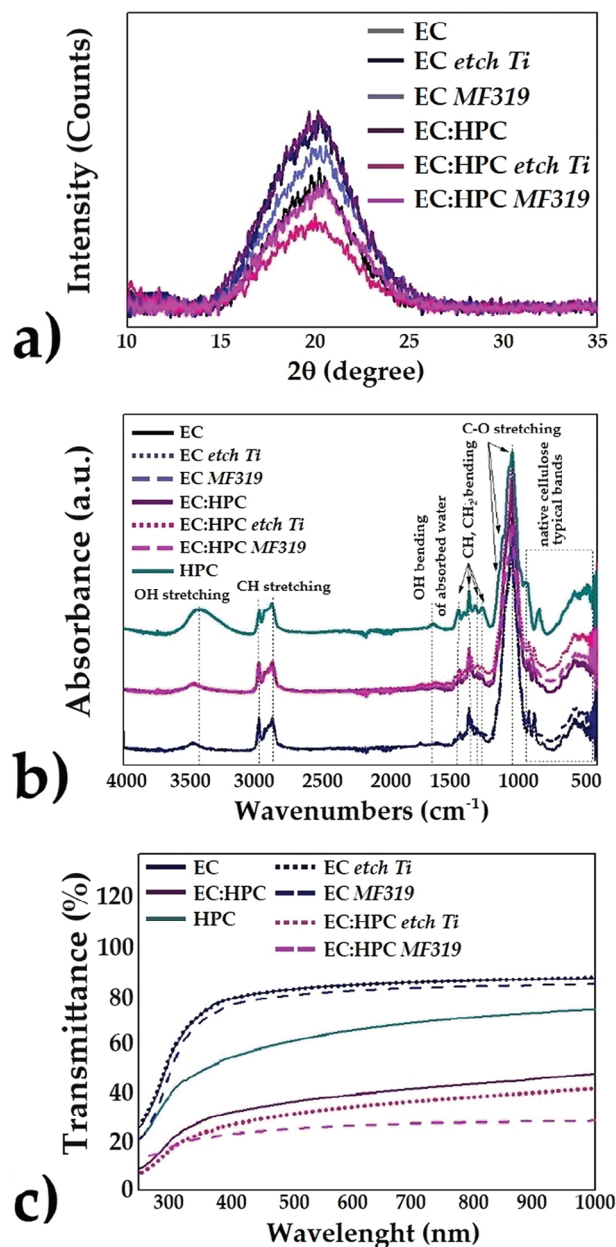
Figure 3. a) XRD diffractogram of EC and EC:HPC substrate pristine and treated with MF319 and Titanium etching solution. b) FTIR-ATR spectra of EC and EC:HPC substrates treated with Titanium etching solution and MF319 developer; c) UV–vis spectra of EC and EC:HPC substrates treated with Titanium etching solution and MF319 developer

EC (hydrophobic), as expected. Significant variations from the EC pristine substrate are not present in the low frequencies' regions for the EC (treated with the MF319), and no changes can be found for the Titanium etching solution. The peak at 1650 cm^{-1} is unaffected by the treatments. Variation in the EC:HPC substrates spectra in the cellulose "fingerprint" region are detected both for the Titanium etching and the MF319.

Despite the alterations observed in the spectra, the EC:HPC substrate shows only a faint sign of oxidation (increase of

ADVANCED
SCIENCE NEWS
www.advancedsciencenews.com

ADVANCED
MATERIALS
TECHNOLOGIES
www.advmattechnol.de

Figure 4. Titanium and Aluminum strain-gauge sensors realized through photolithography on EC and EC:HPC substrates. Titanium capacitive sensor on EC:HPC substrate. In the details section: optical microscope images of Aluminum and Titanium patterns, and a sketch of the capacitive device.

intensity of the 1750 cm^{-1} peak associated with C=O groups) and no unsaturated carbonyl groups are observed at 1660 cm^{-1}. Moreover, no variation of the 3400 cm^{-1} peak is observed, suggesting no modification of the hydroxyl groups of the glucose unit. The results, therefore, confirmed what expected from EC substrate. In fact, EC films and EC powder are inert in aqueous alkalis and resistant to salt solutions, and to oxidation below their softening temperature, which is over 130 °C. However, it is less inert to oxidating acids.[77]

UV–vis transmission analysis of the three different type of cellulose aimed at investigating the transmittance of such substrates (Figure 3c). Measurements have been acquired at room temperature without using the integrating sphere with a wavelength interval of 4 nm. Having used substrates with slightly different thickness (ranging from 100 to 140 µm), and not utilizing the integrating sphere, only qualitative information can be derived, regardless the specific level of transmittance. In any case, as expected, the trend is monotonically decreasing toward UV wavelengths and the EC:HPC sample has a general lower transmittance due to the presence of different domains in the matrix. Various samples and various portions of the same sample were analyzed. It was noted that the reproducibility of EC and HPC substrates its higher (variations among spectra are within the 2% of transmittance), while a greater error was noted for the EC:HPC samples. This could be attributed to the patterned surface, which is responsible of values with an error ≈5%. After treating the samples with MF319 and the etching solution for Titanium, some considerations are to be made. As suggested from the visual observation of the samples, while EC substrates do not exhibit any significant variation in their color, and thus their spectra. On the other hand, the EC:HPC substrate showed a significative decrease in transmittance, which is related to its whitening. This effect can be likely due to the hydration/functionalization of the hydrophilic domains of the substrate.
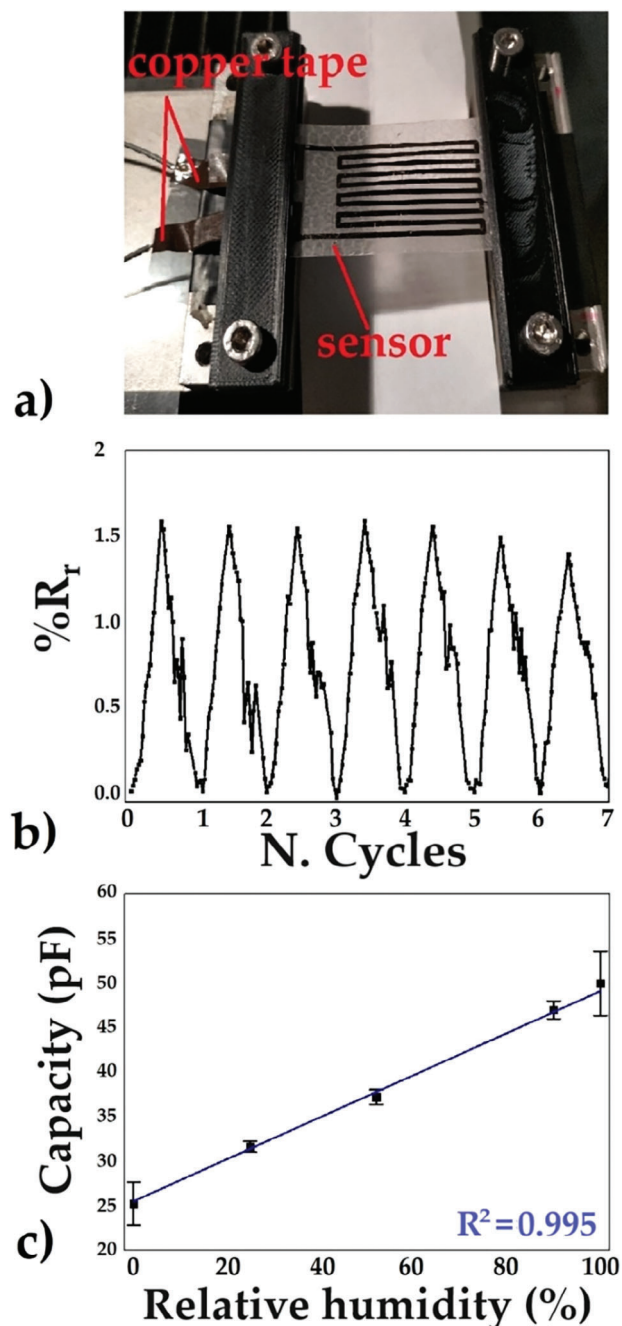
Given all the tests performed, both mechanical and chemical, we proved that it is possible to modulate the mechanical and chemical properties of these self-standing cellulose films by varying the formulation. HPC gives the film a better flexibility and elasticity, at the expense of chemical stability. On the other hand, EC self-standing films are extremely stable from the chemical point of view but are less flexible and tend to crack and break when subjected to minor mechanical stress. The mixed layer, EC:HPC, may represent a good compromise in terms of mechanical properties and chemical stability, being able to withstand fabrication process while enduring thousands of bending cycles.

2.3. Devices Fabrication and Characterization

We successfully managed to validate the technology fabricating a humidity sensor and a strain gauge sensor on both EC and EC:HPC substrates, using Aluminum and Titanium deposited, respectively, via thermal evaporation and electronic-gun based process. Pictures and optical microscopy images of the resistive and capacitive sensors are reported in **Figure 4**, along with a sketch of the capacitive sensor.

As for the resistive strain-gauge sensors, the electrical resistance is in the range of few kΩ, with good reproducibility among several devices. Preliminary characterization data were obtained performing electromechanical bending tests. The device was clamped to the sample holder and electrical connection were made using copper adhesive tape (**Figure 5a**). Resistance-bending curves for the Titanium sensor on EC and for the Aluminum strain-gauge sensor of EC:HPC are reported in Figure 5b, proving its functioning.

The capacitive humidity sensor was realized sandwiching a layer of EC:HPC (dielectric and sensing layer) with two layers of Titanium, the top electrode, patterned, and the bottom

2301282 (7 of 12)

**ADVANCED
SCIENCE NEWS**

www.advancedsciencenews.com

**ADVANCED
MATERIALS
TECHNOLOGIES**

www.advmattechnol.de

Figure 5. a) Electromechanical bending measures set-up. b) Electrical performances in terms of relative resistance during bending cycles. c) Capacity a function of relative humidity (RH).

electrode, common. By doing so, it is possible to have multiple sensor units with one process (Figure 4). The functioning of the device as humidity sensor is based on the response of the EC:HPC layer toward humidity. In fact, the hydrophilic component of the substrate is highly sensitive to water, and both the thickness and the dielectric constant of the devices changes with water content. Some hypothesized a reduction in the dimension of the HPC layer due to the partial transition of the polymeric chain into a solubilized condensed form.[78] As for our configu-

ration, the shrinking of the EC:HPC layers leads to a decrease in the distance between the two metallic layers. An increase in capacity is likely to be expected, being the capacity inversely proportional to the distance between the metallic layers, according to Equation 4:

$$C = \frac{\epsilon \times S}{d} \tag{4}$$

where S in the surface of the metallic plates, d is their distance and ϵ is the dielectric constant of the dielectric layer. The device was exposed to different RH conditions and the capacity was recorded using an impedance analyzer. The response was linear as observed in the graph reported in Figure 5c, with a sensitivity of ≈ 0.24 pF/RH% though presenting higher variability at extreme humidity, due to the significative hydration undergone by the EC:HPC layer.

3. Conclusion

This study introduces a remarkable breakthrough in the production of sustainable, biocompatible, and flexible substrates for electronics. By harnessing the potential of a cost-effective raw material, we have achieved the fabrication of flexible substrates without resorting to time-consuming and energy-intensive procedures. Through a simple, one-step process, utilizing ethanol-based cellulose dispersions, self-standing substrates were produced with no waste of materials or solvents, increasing the efficiency and eco-friendliness of the method.

What sets this research apart is the ability to tailor both the mechanical and chemical properties of the substrates by manipulating the composition of the dispersions. By combining hydrophilic (hydroxypropyl cellulose, HPC) and hydrophobic (ethyl cellulose, EC) cellulose ethers, we demonstrated the versatility of the substrates. Thickness adjustments were effortlessly achieved, with substrates ranging from 60 to ≈ 200 μm.

Mechanical evaluation of the substrates revealed remarkable stability and elongation properties. The HPC substrate exhibited exceptional stability over 2500 bending cycles, coupled with an impressive maximum elongation of 25%. The EC substrate displayed slightly weaker mechanical characteristics but still showed endurance up to 2000 bending cycles for low thickness substrates. The mixed EC:HPC substrate delivered intermediate properties, exhibiting stability over 2500 bending cycles and a relative strain of 3% before breakage.

Furthermore, the processability of these substrates was explored, focusing on their compatibility with standard and very scalable microelectronic fabrication processes such as UV photolithography. The deposition of metallic contacts (Aluminum and Titanium) and the successful fabrication of resistive strain-gauge sensors and a capacitive humidity sensor demonstrates the immense potential of these substrates in electronic device manufacturing. Notably, the use of a biodegradable biopolymer substrate in these processes marks a significant advancement toward environmentally-friendly manufacturing of devices.

The implications of this research are vast and impactful, spanning fields like medical devices (e.g., Titanium-based implants), environmental monitoring, precision agriculture, and biosensors. By revolutionizing the processing of cellulose-based
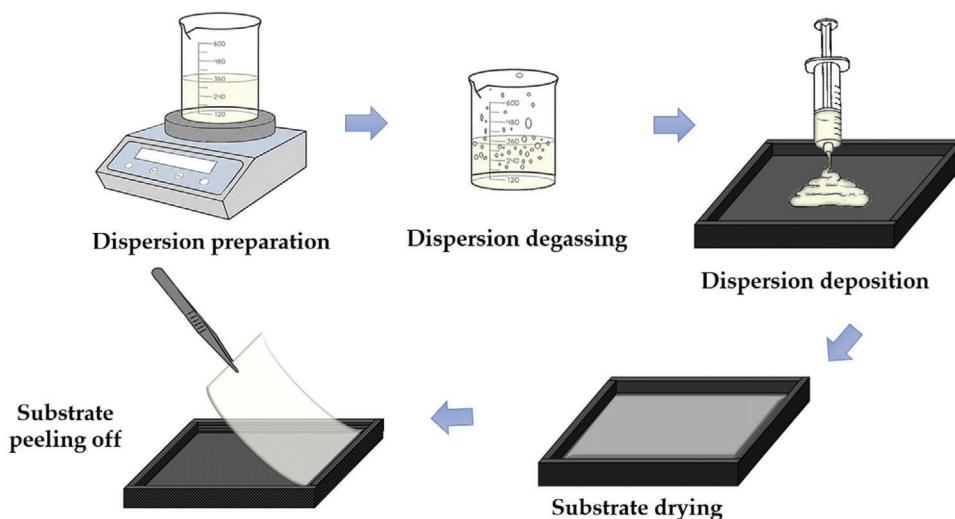
**ADVANCED
SCIENCE NEWS**

www.advancedsciencenews.com

**ADVANCED
MATERIALS
TECHNOLOGIES**

www.advmattechnol.de

Figure 6. Substrates Fabrication Steps.

substrates, this study paves the way for technological innovation and opens up exciting opportunities for the development of cutting-edge electronic devices in various sectors.

4. Experimental Section

Materials: Hydroxypropyl cellulose (HPC) with MW ≈80.000 Da was purchased from Sigma. Ethyl cellulose (EC) with 48–49.5% ethoxy content was purchased from Sigma. All the solvents used were purchased from Sigma. The Aluminum etching solution was a lab prepared mixture of acids composed of 80% orthophosphoric (14.615 м), 5% acetic (17.4 м), and 5% nitric acid (14 м) in deionized water. The Chromium etching solution is composed of ammonium cerium nitrate and perchloric acid and was provided by OSC OrganoSpezialChemic GmbH. The Titanium etching solution is an aqueous 2.84 м HF solution. HF was provided by J.T.Baker. The AZ400K is an aqueous potassium hydroxide solution and was provided by AZ Electronic Materials GmbH. MF319 developer is based on tetramethyl ammonium hydroxide and was provided by ROHM HAARS.

Preparation of the Substrates: The self-standing films were prepared via solvent casting, at room temperature and controlled RH (50%), from ethanol-based solutions. More specifically, three formulations were tested: ethyl cellulose (EC) (10% w/v), ethyl cellulose mixed with hydroxypropyl cellulose (EC:HPC) (7.5%+2.5% w/v) and hydroxypropyl cellulose (HPC) (10% w/v). HPC dispersion (10% w/v) was prepared by dispersing the polymer, as received, in ethanol, manually stirred and left to rest for 24 h.

The mixed EC:HPC dispersion was prepared by dispersing EC and HPC in ethanol and stirring at 35 °C until complete dissolution. EC dispersion was prepared by dissolving it in ethanol and stirring at 45 °C until dissolution.

After a degassing step, the polymeric dispersions were then solvent cast in a mold, with the aid of a syringe, and dried at room temperature overnight. To achieve custom-shaped and reproducible films, 3D-printed ABS molds were realized. They were covered with an adhesive Teflon film, to ease the detachment of the cellulose film, and they had 2 mm high walls, to prevent the cellulose solutions from overflowing. Once dried, the self-standing cellulose films are peeled off from the mold. The main steps are reported in **Figure 6**.

The thickness of the films could be adjusted, within certain limits, by modifying the volume of solution deposited in the mold. More specifically, films with different thickness were studied for each formulation and classified the films according to their thickness as reported in **Table 2**.

Films with thicknesses below 50 µm for the EC:HPC substrate and below 80 µm for EC were not analyzed. These limits were set because preparing thinner films becomes challenging due to the small volume required and increased fragility of the obtained film, especially for EC-based formulations, which compromised their handling and processability. In the case of HPC, films thinner than 80 µm lose their overall rigidity and tend to fold, although remaining flexible and resilient.
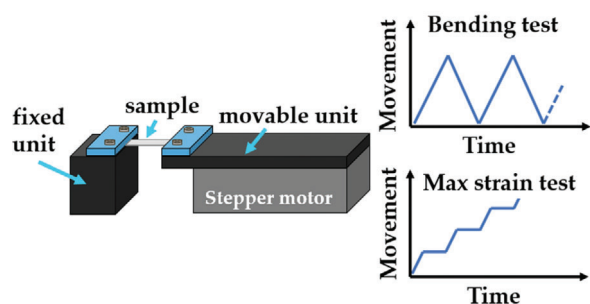
Conversely, the upper end of the thickness range was also explored, investigating thicknesses of up to 160 µm for all samples, despite attempts to prepare thicker samples with all formulations. Specifically, HPC and EC:HPC reached a maximum thickness of ≈220 µm, while for EC alone, it reached ≈180 µm. Notably, the increased thickness had no impact on the bendability of HPC, but it significantly increased the brittleness of EC, making it more challenging to handle and utilize. However, when it comes to EC:HPC, it can be easily managed up to 200 µm in thickness.

Electrode Patterning Process: Interdigitated devices had been fabricated on EC and EC:HPC substrates according to the following procedure: at first, the cellulose sample had been processed in a reactive ion etching system (RIE) with a plasma of Oxygen to clean the surface and to promote the adhesion of the metal layer.

For the fabrication of Aluminum pattern, a thin layer of 100 nm of Al had been deposited through thermal evaporation at ≈10 Å s^{-1}. No crack on either metal film or polymer was detected at this stage, confirming that the sample can withstand the temperature gradient with the evaporation boat. The patterning of the metal has been performed according to standard photolithographic processes: 1) a layer of 1813 positive photoresist, 1.3 µm thick, had been deposited through spin-coating process; 2) soft-bake of the resist had been performed at lower temperature for longer times to save the sample from excessive thermal stress (5 min at 80 °C vs 2 min at 105 °C); 3) EVG610 mask alignment system had been used

Table 2. Classification of cellulose-based films according to their thickness.

	THICKNESS (µm)		
	EC	EC:HPC	HPC
A		50–60	
B	80-100	61-100	80-100
C	101-120	101-120	101-120
D	121-140	121-140	121-140
E	141-160	141-160	141-160

2301282 (9 of 12)

**ADVANCED
SCIENCE NEWS**

www.advancedsciencenews.com

**ADVANCED
MATERIALS
TECHNOLOGIES**

www.advmattechnol.de

Figure 7. Set-up for the mechanical characterization of the cellulose thin films.

to perform pattern definition though UV exposition (100 mJ dose); 4) resist development and Aluminum etching have been performed both using MF319 alkaline developer (total immersion time: 10 min).

For the fabrication of Titanium pattern, a thin layer of 70 nm of Ti was deposited through thermal e-gun evaporation at ≈ 3 Å s^{-1}. The fabrication process was similar to the one for the manufacturing of the Al device (thermal evaporation – 10 Å s^{-1}) except for the Titanium etching performed with the Titanium etching Solution (aqueous HF solution) for 5 s.

The capacitive sensor was realized on the EC:HPC substrate, depositing 70 nm of Titanium on both sides and then defining through photolithographic process 1×1 cm^2 squares on the top layer.

Characterization Techniques: Rheological characterization was performed using an AR 2000 rheometer by TA Instruments. A cone and plate set-up (cone with 60 mm diameter 2°, acrylic) was used. Flow measurements were performed testing a range from 0.01 to 1000 s^{-1}. All experiments were performed at room temperature. The tests were repeated multiple times with samples coming from different batches, and in all cases the results were reproduced within a maximum difference of 10%. Errors are not reported in the graphs presented for the sake of clarity, and they do not affect the hierarchy of the displayed parameters.

The thickness of the films was measured using a feeler gauge, DIGI-MATIC INDICA-TOR by Mitutoyo, able to measure thicknesses from 1 μm up to 1 mm.

Morphology characterization was performed via scanning electron microscopy using a FE-SEM (Sigma 300 Carl Zeiss).

XRD measurements were performed in a Bruker D8 Discover diffractometer equipped with a Cu X-ray source (Cu-kα1 radiation $\lambda = 1.54$ Å, 40 kV, and 40 mA) in a 2θ-ω out-of- plane high resolution configuration.

UV–vis spectroscopy was performed using a Perkin Elmer Lambda 35 UV/vis spectrometer. The spectra were collected from 1100 to 200 nm with a resolution of 4 nm.

FTIR-ATR characterization was performed using a ThermoScientific Nicolet Summit spectrometer in absorbance mode. Samples were measured in attenuated total reflectance mode (ATR), with a diamond crystal with single reflection accessory. The spectra were collected from 4000 to 400 cm^{-1} with a resolution of 2 cm^{-1}.

Mechanical characterization was performed using a motorized linear stepping motor by Newport sp300. The thin flexible films were cut into 5×0.5 cm^2 samples and mounted on the linear trail motioned by a Newport sp300 stepper motor, as shown in **Figure 7**. The samples were pulled between the two ends, one fixed and one mobile, at a fixed speed (2 mm min^{-1}).

The motor is driven by custom software made in LabView, which controls the advance and retraction of the movable holder. Electromechanical characterizations were performed at room temperature using the same set-up reported in Figure 7, however for these measurements the sample's resistance was monitored with a Keithley 2440 Multimeter interfaced with the same custom software. The capacity was measured with a HP4192 Impedance Analyzer using a signal of 50 mV @1 kHz. All the characterizations were performed at room temperature.

Supporting Information

Supporting Information is available from the Wiley Online Library or from the author.

Conflict of Interest

The authors declare no conflict of interest.

Author Contributions

E.P., F.M., L.M. performed conceptualization; E.P., F.M., L.M., A.D.F., and I.L. performed acquisition, analysis or interpretation of data; E.P., F.M., and L.M. wrote and prepared the original draft; E.P., F.M., L.M., E.T., R.C., and S.O. wrote the original draft and reviewed and edited the final manuscript; F..M. and L.M. performed the supervision. All authors have read and agreed to the published version of the manuscript.

Data Availability Statement

The data that support the findings of this study are available from the corresponding author upon reasonable request.

[1] R. Cancelliere, D. Albano, B. Brugnoli, K. Buonasera, G. Leo, A. Margonelli, G. Rea, *Appl. Surf. Sci.* **2021**, *567*, 150791.

[2] A. Pecora, L. Maiolo, M. Cuscunà, D. Simeone, A. Minotti, L. Mariucci, G. Fortunato, *Solid. State. Electron.* **2008**, *52*, 348.

[3] J. Park, N. Choudhary, J. Smith, G. Lee, M. Kim, W. Chois, *Appl. Phys. Lett.* **2015**, *106*, 012104.

[4] L. Maiolo, A. Pecora, F. Maita, A. Minotti, E. Zampetti, S. Pantalei, A. Macagnano, A. Bearzotti, D. Ricci, G. Fortunato, *Sensors Actuators B Chem.* **2013**, *179*, 114.

[5] K. Sangmo, V. Q. Hoang, B. C Wung, *Mater. Today Energy* **2021**, *19*, 100583.

[6] R. Cancelliere, A. Di Tinno, A. M. Di Lellis, G. Contini, L. Micheli, E. Signori, *Biosens. Bioelectron.* **2022**, *213*, 114467.

[7] L. Maiolo, A. Ferraro, F. Maita, R. Beccherelli, E. E. Kriezis, T. V. Yioultsis, D. C. Zografopoulos, *Appl. Phys. Lett.* **2019**, *115*, 241602.

[8] Y. S. Kim, *Sensors Actuators B Chem.* **2006**, *114*, 410.

[9] L. Frisk, S. Lahokallio, J. Kiilunen, K. Saarinen-Pulli, *MRS Adv* **2016**, *1*, 3477.

[10] Plastic Europe PEMRG, *Assoc. Plast. Manuf.* **2017**.

[11] HD Microsystems, *SDS PI 2611.* **2018**.

[12] B. Zhu, H. Wang, W. R. Leow, Y. Cai, X. J. Loh, M. Y. Han, X. Chen, *Adv. Mater.* **2016**, *28*, 4250.

[13] E. Palmieri, L. Montaina, G. Polino, M. Bonomo, G. Giordanengo, C. Barolo, G. Paradossi, F. Brunetti, E. Tamburri, S. Orlanducci, *Appl. Surf. Sci.* **2023**, *608*, 155117.

[14] X. Liu, W. Xiao, T. Tao, J. Yang, H. Li, Q. Chen, L. Huang, Y. Ni, L. Chen, X. Ouyang, X. Zhu, J. Li, *Carbohydr. Polym.* **2021**, *260*, 117820.

[15] R. Taguchi, N. Akamatsu, K. Kuwahara, K. Tokumitsu, Y. Kobayashi, M. Kishino, K. Yaegashi, J. Takeya, A. Shishido, *Adv. Mater. Interfaces* **2021**, *8*, 2001662.

[16] H. Shin, J. Roh, J. Song, H. Roh, C. M. Kang, T. Lee, G. Park, K. An, J. Y. Kim, H. Kim, J. Kwak, C. Lee, H. Kim, *Adv. Mater. Interfaces* **2019**, *6*, 1801731.

[17] F. Brunetti, A. Operamolla, S. Castro-Hermosa, G. Lucarelli, V. Manca, G. M. Farinola, T. M. Brown, F. Brunetti, S. Castro-Hermosa, G. Lucarelli, V. Manca, T. M. Brown, A. Operamolla, G. M. Farinola, *Adv. Funct. Mater.* **2019**, *29*, 1806798.

[18] S. Castro-Hermosa, J. Dagar, A. Marsella, T. M. Brown, *IEEE Electron. Device Lett.* **2017**, *38*, 1278.

[19] L. Leonat, M. S. White, E. D. Głowacki, M. C. Scharber, T. Zillger, J. Rühling, A. Hübler, N. S. Sariciftci, *J. Phys. Chem. C* **2014**, *118*, 16813.

[20] E. P. Hoppmann, W. W. Yu, I. M. White, *Methods* **2013**, *63*, 219.

[21] L. L. Qu, Q. X. Song, Y. T. Li, M. P. Peng, D. W. Li, L. X. Chen, J. S. Fossey, Y. T. Long, *Anal. Chim. Acta* **2013**, *792*, 86.

[22] D. Nilsson, T. Kugler, P. O. Svensson, M. Berggren, *Sensors Actuators, B Chem.* **2002**, *86*, 193.

[23] S. Ge, L. Ge, M. Yan, X. Song, J. Yu, J. Huang, *Chem. Commun.* **2012**, *48*, 9397.

[24] D. D. Liana, B. Raguse, L. Wieczorek, G. R. Baxter, K. Chuah, J. J. Gooding, E. Chow, **2013**, *3*, 8683.

[25] L. Ma, R. Liu, H. Niu, M. Zhao, Y. Huang, *Compos. Sci. Technol.* **2016**, *137*, 87.

[26] J. Liang, C. Jiang, W. Wu, *Nanoscale* **2019**, *11*, 7041.

[27] G. Polino, A. Scaramella, V. Manca, E. Palmieri, E. Tamburri, S. Orlanducci, F. Brunetti, *Energy Technol.* **2020**, *8*, 1901233.

[28] Y. Sun, D. Chen, Y. Li, S. Sun, J. Zheng, J. Cui, G. Wang, L. Zheng, Y. Wang, H. Zhou, *Carbohydr. Polym.* **2021**, *270*, 118359.

[29] T. G. Majewicz, P. E. Erazo-Majewicz, T. J. Podlas. Cellulose Ethers in EPSE 2nd ed., Vol. 3, pp. 226. https://doi.org/10.1002/0471440264.PST044.

[30] B. Andres, C. Dahlström, N. Blomquist, M. Norgren, H. Olin, *Mater. Des.* **2018**, *141*, 342.

[31] D. Zhao, Y. Zhu, W. Cheng, W. Chen, Y. Wu, H. Yu, D. Y. Zhao Zhu, W. Cheng, W. Chen, H. Yu, D. Zhao, Y. Wu, *Adv. Mater.* **2021**, *33*, 2000619.

[32] A. Rivadeneyra, A. Marín-Sánchez, B. Wicklein, J. F. Salmerón, E. Castillo, M. Bobinger, A. Salinas-Castillo, *Compos. Sci. Technol.* **2021**, *208*, 108738.

[33] G. Ayissi Eyebe, B. Bideau, N. Boubekeur, É. Loranger, F. Domingue, *Sensors Actuators, B Chem.* **2017**, *245*, 484.

[34] Y. Zhu, Y. Guo, K. Cao, S. Zeng, G. Jiang, Y. Liu, W. Cheng, W. Bai, X. Weng, W. Chen, D. Zhao, H. Yu, Y. Guihua, *Nat. Synth.* **2023**, *9*, 864.

[35] J. Geyuan, W. Gang, Z. Ying, C. Wanke, C. Kaiyue, X. Guangwen, Z. Dawei, Y. Haipeng, *Research* **2022**, *2022*, 9814767.

[36] Z. Dawei, Z. Ying, C. Wanke, X. Guangwen, W. Qingwen, L. Shouxin, L. Jian, C. Chaoji, Y. Haipeng, H. Liangbing, *Matter* **2020**, *2*, 390.

[37] S. Stelzl, *Microscale 2D and 3D Photolithography of Cellulose Nanocrystal Composites*, Technische Universität Wien, Vienna, Austria **2020**.

[38] A. Wolfberger, A. Petritz, A. Fian, J. Herka, V. Schmidt, B. Stadlober, R. Kargl, S. Spirk, T. Griesser, *Cellulose* **2015**, *22*, 717.

[39] S. Verma, Gaganjot, J. T, M. Katiyar, V. Verma, *Appl. Mater. Today* **2018**, *13*, 83.

[40] D. J. Gundlach, H. Klauk, C. D. Sheraw, C.-C. Kuo, J.-R. Huang, T. N. Jackson, *Int. Electron Devices Meet 1999, 1999. Techical Digest*, IEEE, Piscataway, NJ **1999**.

[41] S. M. C. Francis, S. Gray, D. Struchen, S. Malfoy, Y. Darbellay, N. Magnon, B. Le Gratiet, J.-C. Tisserand, *Proc. SPIE 3099, Micro-optical Technol. Meas. Sensors, Microsystems II Opt. Fiber Sens. Technol. Appl.* **1997**, https://doi.org/10.1117/12.281232.

[42] E. Akçalı, K. Nemoto, R. Uzsoy, *IEEE Trans. Semicond. Manuf.* **2001**, *14*, 48.

[43] D. Adams, Z. Ounaies, A. Basak, *JOM* **2021**, *73*, 3761.

[44] S. Kim, H. Lee, D. Kim, H. Ha, N. Qaiser, H. Yi, B. Hwang, *Surf. Coatings Technol.* **2020**, *394*, 125898.

[45] J. Xiong, S. Li, Y. Ye, J. Wang, K. Qian, P. Cui, D. Gao, M.-F. Lin, T. Chen, P. See Lee, J. Q. Xiong, S. H. Li, J. X. Wang, K. Qian, P. Cui, D. C. Gao, M. Lin, P. S. Lee, Y. Y. Ye, T. P. Chen, *Adv. Mater.* **2018**, *30*, 1802803.

[46] J. W. Phair, *J. Am. Ceram. Soc.* **2008**, *91*, 2130.

[47] P. Ahmadi, A. Jahanban-Esfahlan, A. Ahmadi, M. Tabibiazar, M. Mohammadifar, *Food Rev. Int.* **2020**, *38*, 685.

[48] A. S. Sharova, F. Modena, A. Luzio, F. Melloni, P. Cataldi, F. Viola, L. Lamanna, N. F. Zorn, M. Sassi, C. Ronchi, J. Zaumseil, L. Beverina, M. R. Antognazza, M. Caironi, *Nanoscale* **2023**, *15*, 10808.

[49] L. Lamanna, G. Pace, I. K. Ilic, P. Cataldi, F. Viola, M. Friuli, V. Galli, C. Demitri, M. Caironi, *Nano Energy* **2023**, *108*, 108168.

[50] B. R. Giri, S. Poudel, D. W. Kim, *J. Pharm. Investig.* **2020**, *51*, 1.

[51] Y. M. Than, S. Suriyarak, V. Titapiwatanakun, *Polymers (Basel)* **2022**, *14*, 1108.

[52] L.-S. Ebers, M.-P. Laborie, *Cite This ACS Appl. Bio Mater* **2020**, *2020*, 6907.

[53] E. Palmieri, F. Pescosolido, L. Montaina, R. Carcione, G. Petrella, D. O. Cicero, E. Tamburri, S. Battistoni, S. Orlanducci, *Gels* **2022**, *8*, 783.

[54] E. B. Gutoff, E. D. Cohen, *Coating and Drying Defects: Troubleshooting Operating Problems*, 2nd Edition, Wiley, Hoboken. USA **2006**.

[55] R. D. Hester, D. R. Squire, *J. Coatings Technol.* **1997**, *69*, 109.

[56] U. Siemann, in *Progress in Colloid and Polymer Science Scatt. Methods Prop. Polym. Mater.*, (Eds.: F. Kremer, W. Richtering, N. Stribeck, B. Smarsly), Springer Verlag, Berlin, Germany **2005**, 130, pp. 1.

[57] P. Takkalkar, M. J. Tobin, T. Vongsvivut, S. Nizamuddin, G. Griffin, N. Kao, *J. Taiwan Inst. Chem. Eng.* **2019**, *104*, 293.

[58] V. Carnicer, C. Alcázar, M. J. Orts, E. Sánchez, R. Moreno, *Open Ceram* **2021**, *5*, 100052.

[59] C. W. Macosko, **1994**.

[60] H. L Hernandez, J. W. Souza, E. A. Appel, *Macromol. Biosci.* **2021**, *21*, 2000295.

[61] H. F. Giles, J. R. Wagner, M. M. Eldridge, *Extrusion, The Definitive Processing Guide and Handbook, Plastic Design Library.*, William Andrew, Inc, Norwich, NY **2014**.

[62] M. Kontopoulou, Applied polymer rheology:polymemeric fluids with industrial applications. John Wiley & sons **2011**, 354.

[63] G. Campbell, M. Spalding, in *Trubleshooting Anal. Single-Screw Extrus*, Hanser Publications, xx **2013**, pp. 57–108.

[64] H.-I. Hsiang, C.-C. Chen, L.-F. Fan, H.-Y. Cheng, *Curcuit World* **2020**, *47*, 43.

[65] K. Inukai, Y. Takahashi, K. Ri, W. Shin, *Ceram. Int.* **2015**, *41*, 5959.

[66] A. Santamaría, M. I. Lizaso, M. E. Muñoz, *Macromol. Symp.* **1997**, *114*, 109.

[67] M. M. Cross, *J. Colloid Sci.* **1965**, *20*, 417.

[68] Y. Song, Q. Zheng, *J. Rheol.* **2015**, *59*, 155.

[69] P. Navard, J. M. Haudin, *J. Polym. Sci. Part B Polym. Phys.* **1986**, *24*, 189.

[70] M. Osterhold, *Prog. Org. Coatings* **2000**, *40*, 131.

[71] T. Heinze, Omar A. El Seoud, A. Koschella, **2018**, 293.

[72] S. Park, J. O. Baker, M. E. Himmel, P. A. Parilla, D. K. Johnson, *Biotechnol. Biofuels* **2010**, *3*, 10.

**ADVANCED
SCIENCE NEWS**

www.advancedsciencenews.com

**ADVANCED
MATERIALS
TECHNOLOGIES**

www.advmattechnol.de

[73] X. Ju, M. Bowden, E. E. Brown, X. Zhang, *Carbohydr. Polym.* **2015**, *4*, 476.

[74] M. Trivedi, A. Branton, D. Trivedi, G. Nayak, R. Mishra, S. Jana, *Int. J. Biomed. Mater. Res.* **2015**, *3*, 83.

[75] F. Paulo, L. Tavares, L. Santos, *J. Food Meas. Charact.* **2022**, *16*, 3077.

[76] N. Halib, M. Amin, M. C. Iqba, I. Ahmad, *Sains Malaysiana* **2012**, *41*, 205.

[77] D. Cellulosics, *ETHOCEL Ethylcellulose Polymers Techincal Handbook*, Dow Chemical Company, Michigan, USA **2005**.

[78] M. Seo, E. Kumacheva, *Colloid Polym. Sci.* **2002**, *280*, 607.